AURORAL KILOMETRIC RADIATION SOURCE REGION VARIATIONS WITH SEASON AND SOLAR CYCLE

L. N. Garcia*, J. L. Green†, S. A. Boardsen‡, S. F. Fung† , and B. W. Reinisch§

Abstract

Data from the Imager for Magnetopause-to-Aurora Global Exploration (IMAGE) and the Polar plasma wave instruments were used to study the seasonal and solar cycle variations of the northern hemisphere auroral kilometric radiation (AKR) source region. Our results show that there are significant seasonal changes in the AKR spectrum. We find that the spectral peak drifts from ∼260 kHz in the winter to ∼150 kHz in the summer and the overall intensity is weaker. Assuming that the AKR is generated by means of the cyclotron maser mechanism this implies that the AKR source region (the auroral density cavity) moves to higher altitudes during the summer months. Data from the DE-1 plasma wave instrument were used to study the seasonal variation of the AKR region in magnetic local time (MLT). During the winter months the MLT range of the AKR region extends from 18–24 MLT with a source centroid near ∼20 MLT. During the summer months the MLT range narrows to 20–24 MLT and the source centroid moves closer to ∼22 MLT. Comparing Polar and IMAGE data also allowed for an analysis of the solar cycle variations of the AKR. The average AKR spectrum is typically weaker by about an order of magnitude during solar maximum. These results illustrate that variations in ionospheric density with solar EUV flux both seasonally and with solar cycle have significant effects on the AKR source region due to strong magnetospheric-ionospheric coupling. The effect of this coupling is that increases in ionospheric density result in a narrowing of the altitude and magnetic latitude range of the AKR density cavity and a decrease in the intensity of AKR by lessening the density depth of the auroral density cavity. These results will need to be accounted for in any development of an AKR-related substorm index and for statistical studies of the AKR emission pattern.

* *QSS Group, Inc./NASA/GSFC, Greenbelt, USA*
† *NASA Goddard Space Flight Center, Greenbelt, MD, USA*
‡ *L-3 Communications, Government Services, Inc., Greenbelt, USA*
§ *Center for Atmospheric Research, University of Massachusetts, Lowell, USA*

1 Introduction

In the kilometer wavelengths, Earth is a powerful radio planet [Gurnett, 1974; Kaiser and Stone, 1975; Zarka, 2000]. Benediktov et al. [1968] noted that the intensity of sporadic emissions at 725 and 1100 kHz correlated well with the Kp geomagnetic activity index. Dunckel et al. [1970] found that their "highpass emissions" observed by OGO–1 were well correlated with the auroral electroject index (AE) and were most commonly seen over the midnight sector. Gurnett [1974] and Kurth et al. [1975] further showed that this auroral kilometric radiation (AKR) originates at low altitudes ($< 3R_E$), spans the frequency range of approximately 50–500 kHz and is associated with discrete auroral arcs on the Earth's nightside. Voots et al. [1977] investigated using AKR as a measure of auroral disturbances, comparing AKR power flux to the AE index. The authors noted a good correlation between Imp 6 AKR measurements at 178 kHz and AE. With higher AE values ($> 100\gamma$) however the proportionality constant between AKR and AE changed. This change was explained by noting that the spectral peak of AKR moves to lower frequency with higher AE [Kaiser and Alexander, 1977] increasing the power in the 178 kHz channel. Spacecraft measurements of AKR however are also strongly influenced by beaming and propagation effects especially for low latitude spacecraft on the Earth's dayside [Green et al., 1977]. Murata et al. [1997] and Kurth and Gurnett [1998] using data from Geotail and Polar spacecraft respectively, developed indices based on the AKR power emitted across the entire AKR spectrum. This would take into account the drift in the spectral peak with magnetic activity and should more accurately reflect the strength of the substorm activity. When both spacecraft were within the emission cone the indices showed good agreement and both compared well with AE [Kurth et al., 1998].

Recent results have shown that seasonal and solar cycle variations in ionospheric density can also have a strong influence on the intensity and spectral distribution of AKR [Green et al., 2004]. Kasaba et al. [1997] using Geotail data and Kumamoto and Oya [1998] using Akebono data found evidence that AKR is more active in the winter polar regions than in the summer polar regions. This effect was more pronounced near the high frequency portion of the AKR spectrum. Kumamoto et al. [2003] have shown that the vertical distribution of the occurrence probability of AKR varies both with season and with solar cycle. Since refraction effects can be significant when observing AKR especially at the higher frequencies and these effects would also be enhanced by ionospheric density increases it is important to distinguish possible propagation effects from changes in the source region itself.

Wu and Lee [1979] proposed a cyclotron maser instability (CMI) mechanism for the generation of AKR. This requires both a source of free energy in the electron distribution and very low densities for the local cold electron background. ISIS 1 observations found the AKR source region to coincide with regions of depleted electron density, satisfying this second requirement [Benson and Calvert, 1979, Calvert, 1981]. That the AKR emission frequency is very near the local electron gyrofrequency, [see e.g. Hilgers et al., 1991] in the auroral density cavity where the electron distribution function has many sources of free energy [Ergun et al., 2000] is strong observational support for the CMI mechanism. The altitude range of the source region can be estimated using the observed AKR spectrum [Lee et al., 1980]. The peak in the AKR spectrum is where the plasma density is the

lowest, maximizing the growth rate for the instability. The AKR spectrum can therefore provide information on the location of the auroral density cavity and acceleration region.

In this article the average spectral characteristics of AKR over both season and solar cycle and over the the entire AKR frequency range will be investigated in order to deduce the changes in extent and location of the auroral density cavity and acceleration region in altitude and local time. This analysis will provide greater insight into the degree of influence the ionosphere has on substorm processes that are initiated in the magnetosphere.

2 Observations

The observations used in this study are from the plasma wave instruments on the polar orbiting Imager for Magnetopause-to-Aurora Global Exploration (IMAGE), Polar, and Dynamics Explorer–1 (DE-1) spacecraft. The IMAGE spacecraft was launched on 25 March 2000 into a highly elliptical polar orbit with initial geocentric apogee of 8.22 Earth radii (R_E) and perigee altitude of 1000 km. The Radio Plasma Imager (RPI) instrument on IMAGE is a highly flexible radio sounder that transmits and receives coded radio frequency pulses in the frequency range from 3 kHz to 3 MHz. RPI also makes passive radio measurements that will be used in this study. RPI utilizes three orthogonal dipole antennas of 325 m (X-axis), 500 m (Y-axis), and 20 m (Z-axis), all tip-to-tip lengths. The X-axis antenna was 500 m at the beginning of the mission but was shortened to 325 m when it apparently collided with a micrometeor or orbital debris on 3 October 2000. For more details on the operation of RPI, see Reinisch et al. [2000]. The Polar spacecraft was launched on 24 February 1996 into a highly elliptical polar orbit with initial perigee and apogee of 2.2 and 9 R_E geocentric radial distance respectively. The plasma wave instrument (PWI) on Polar is designed to measure the electric field from 0.1 Hz to 800 kHz on three antennas. The instrument operated successfully until August 1997. PWI AKR spectral observations used in this study were taken from the long ($\sim$130 meters tip-to-tip) Eu antenna (unless otherwise stated) when the instrument was in the logarithmic sampling mode. For more details on the operations of the Polar/PWI instrument see Gurnett et al. [1995]. DE–1 was launched on 3 August 1981 into a polar orbit (90° inclination) with initial apogee of 4.65 R_E geocentric radial distance and a perigee of 675 km altitude with an orbital period of about 7 hours. The PWI on DE–1 obtained spectral and polarization measurements over a frequency range from 2 Hz to 400 kHz. The DE/PWI electric field measurements used in this study are all from the 200 m tip-to-tip wire antenna. For a more complete description see Shawhan et al. [1981].

3 Seasonal Variations

The AKR spectrum can be investigated for seasonal variations by analyzing the data as a function of dipole tilt angle. Figure 1a is the distribution of AKR as a function of dipole tilt for IMAGE RPI data for times when only AKR is observed in the emission cone [Green et al., 1977]. Times when solar type III radio bursts are observed at the same frequency as the AKR were explicitly excluded from this survey. The number of

AKR spectrums used in Figure 1a varied from a high of over 900 near ±15° dipole tilt to as low as 250 near 0° dipole tilt with the average number of ∼ 500 spectra per 0.7° of dipole tilt bin. A $1/R^2$ correction in the power flux value (normalized to 8 R_E) has been applied to each observation assuming an auroral zone source (22 MLT, 72° invariant latitude) where the wave frequency equals f_g (dipole model). Figure 1 clearly presents two main seasonal effects on the average AKR spectrum: (1) the AKR emission spectrum shifts down in frequency with increasing dipole tilt and (2) the emission spectrum extends over a larger frequency range for negative dipole tilt angles than for positive dipole tilt angles. The change in slope of the data in Figure 1 occurs near 0°. The altitude of the upper (low frequency) boundary of the AKR source appears, on the average, to be the same regardless of positive dipole tilt. However AKR to much lower frequencies have on occasion been observed [Pazamickas, et al., submitted to J. Geophysical Research, 2005]. The altitude of the lower (high frequency) boundary of the region appears to rise slightly with positive dipole tilt. The variation of AKR intensity with dipole tilt seen in this figure will be addressed further in Figure 2. Figure 1b is in the same format as Figure 1a but is the AKR data from the Polar/PWI from March to May 1996 and February to September 1997 when the instrument was connected to the Eu antenna. Although this data set is somewhat limited (no Polar/PWI data is available for the extreme negative dipole tilt angles when PWI was connected to the Eu antenna) it is clear that the average Polar/PWI AKR spectra shows the same trend to lower frequencies with higher dipole tilt as the IMAGE/RPI.

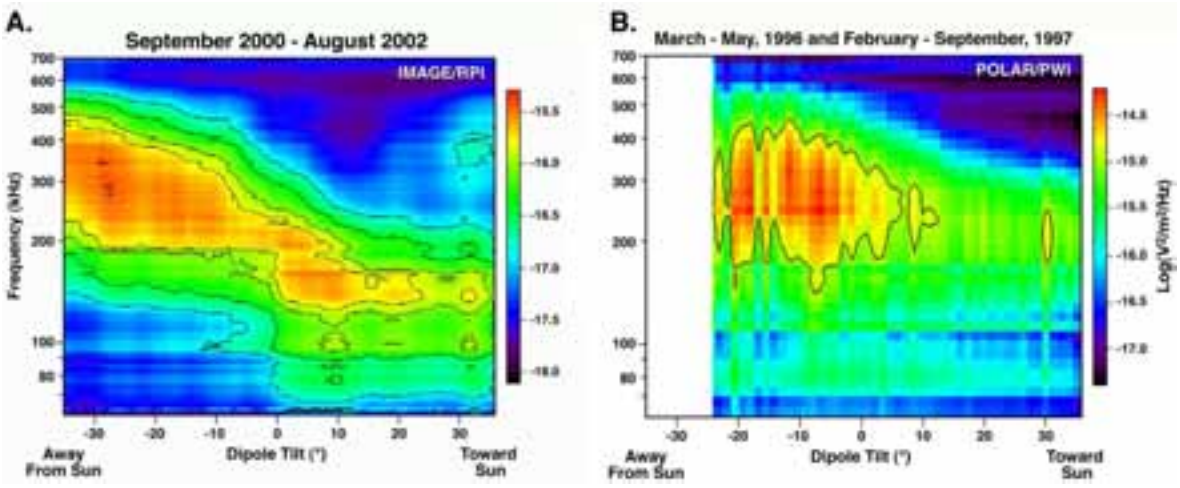

Figure 1: The average spectra of AKR as a function of dipole tilt angle from observations by the IMAGE/RPI instrument (a) and the Polar/PWI instrument (b).

Figure 2 is the average AKR spectrum for positive and negative dipole tilt angles where the emission peak frequency remained approximately constant. For positive tilt angles the emission peak is at ∼150 kHz while for negative dipole tilt angles the emission peak is at ∼260 kHz. The AKR spectrum for negative dipole tilt angles is much broader than for positive tilt angles and it is more intense at the higher frequencies by as much as two orders of magnitude.

Figure 3 is a qualitative illustration of the AKR spectrum mapped into contours of f_p/f_g

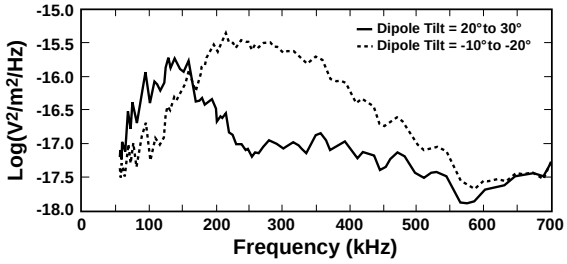

Figure 2: Comparison of the average AKR spectra over dipole tilt extremes where the emission peak is approximately constant.

for a 70° invariant auroral field line using the T96 magnetic field model [Tsyganenko, 1995]. Consistent with the observations presented in Figures 1 and 2, the source region during extreme negative dipole tilt angles (winter) shows the auroral zone density cavity stretching from a region where $f_g = 500$ kHz to nearly $f_g = 80$ kHz. In contrast, for extreme positive dipole tilt angles the source region extent is much smaller, has moved further up the field line, and has a lower frequency boundary of 60 kHz and an upper frequency boundary near 250 kHz.

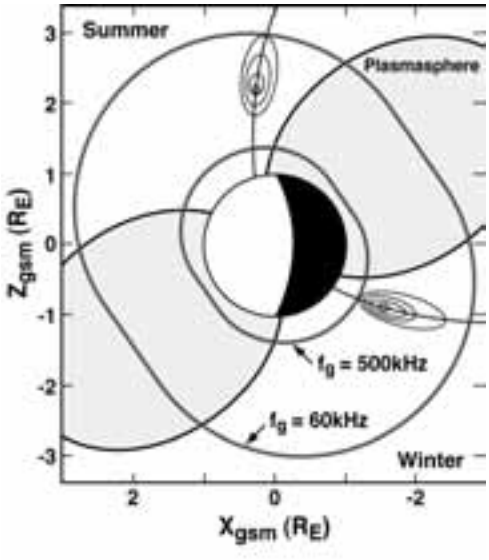

Figure 3: Qualitative contours of f_p/f_g of the auroral density cavity under dipole tilt extremes showing the shift in AKR source region up the field line during the summer and a lower altitude and longer source region during the winter.

The time averaged AKR source location has been determined by Gallagher and Gurnett [1979] to be between 22 and 24 MLT and below 2.5 R_E but at the time of that study no effort was made to investigate any seasonal variation in the source location. On the basis of the dramatic effect dipole tilt angle has on the emission spectrum, and therefore source region altitude, it is essential that variations in the source location in MLT also be investigated. To perform this analysis, the DE/PWI archived data set was chosen because

of the extensive coverage in the AKR source region altitudes, MLT, and over all dipole tilt angles.

Figure 4 is a plot at 186 kHz (near the AKR spectral peak) of all DE/PWI observations from 16 September 1981 through 23 June 1984 when the spacecraft measured a local f_g between 186 to 280 kHz in MLT and invariant latitude. This range in gyrofrequency was chosen to provide adequate statistics where each pixel has more than 50 and as many as 320 observations while balancing smearing of the source region location due to the expected broad emission pattern. Subject to this constraint, the wave amplitudes were binned by magnetic local time, magnetic latitude and by the sign of $Z_{SM} * \psi$, where ψ is the dipole tilt angle and Z_{SM} is the z position of the spacecraft in Solar Magnetic coordinates. The average wave amplitudes derived from this binning, referenced to the Northern hemisphere, are shown in Figure 4. It is important to note that IMAGE/RPI observations (not shown here) show the same trend as the DE/PWI data shown in Figure 4 but with much less statistical confidence.

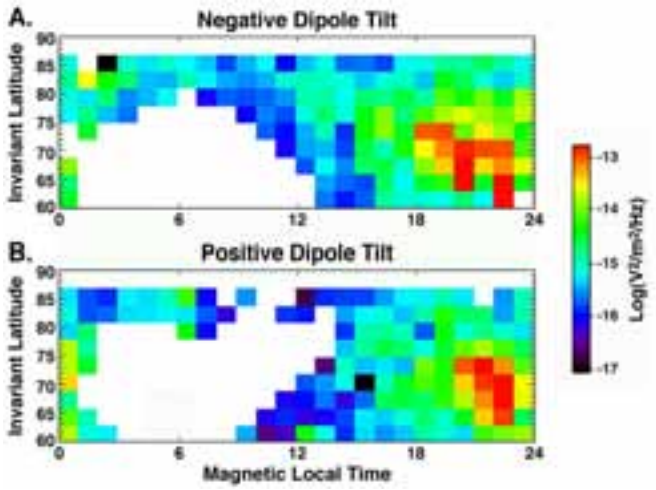

Figure 4: The magnetic local time distribution of the average Northern hemisphere AKR source region from 186 kHz electric field measurements from the DE/PWI for (a) negative and (b) positive dipole tilt angles.

The observations presented in Figure 4 show a clear distinction in the location of the maximum wave intensity with dipole tilt angle (referenced to the Northern Hemisphere). For negative dipole tilt angles (Figure 4a) the AKR source region extends to near dusk with the source centroid near $\sim$20 MLT. For positive dipole tilt angles (Figure 4b) the source region is more confined to 20–24 MLT with the centroid near $\sim$ 22 MLT. It is these latter observations that are more consistent with the Gallagher and Gurnett [1979] results.

4 Solar Cycle Variations

It is well known that EUV and shorter wavelength emissions from the sun greatly intensifies during solar maximum causing a general enhancement in ionospheric densities. On

the basis of the results presented here, it is intriguing to compare the average spectral characteristics of AKR between solar minimum and solar maximum. If ionospheric densities play a major role in the location and depth of the auroral density cavity (the AKR source region), as this study strongly suggests, then we would also expect the average AKR spectrum to exhibit a solar cycle variation with the unexpected result that AKR would be less intense during solar maximum.

Since the Polar plasma wave observations were taken during the last solar minimum and IMAGE plasma wave measurements were taken during the most recent solar maximum a comparison of the average spectra will be used to investigate solar cycle effects. It is not possible to compare simultaneous observations by Polar/PWI and IMAGE/RPI since the former was not operating after the launch of IMAGE. However observations from Polar/PWI and IMAGE/RPI can be compared with Wind/Wave measurements. An in-flight calibration check of the IMAGE/RPI instrument was done by comparing the simultaneous observed power flux measurements of several type III radio bursts with those from the Wind/Waves instrument. A similar analysis was performed between simultaneous Polar/PWI and Wind/Waves instruments of several solar type III radio bursts. Both comparisons showed that these instruments were making measurements that were, at times nearly identical, or within less than 10 db and therefore in reasonable agreement. For details on the Wind/Waves instrument see Bougeret et al. [1995].

In order to investigate solar cycle variations in the AKR spectrum it is now clear that these comparisons can only be valid under the same conditions of dipole tilt angle since significant variations exist with dipole tilt as shown in the previous section. Figure 5 shows the average AKR intensity for (a) positive dipole tilt angles and (b) negative dipole tilt angles. The solid curves are the IMAGE/RPI data taken during solar maximum and the dashed curves are the Polar/PWI data taken during solar minimum. This comparison shows a characteristic decrease in the intensity of AKR over the solar cycle with the AKR intensity typically less by about an order of magnitude during winter seasons during solar maximum. In addition, for positive dipole tilt conditions the AKR spectrum for higher frequencies, observed during solar maximum, is significantly below (by nearly two orders of magnitude) the solar minimum observations for the higher frequency portion of the spectrum (> 200 kHz).

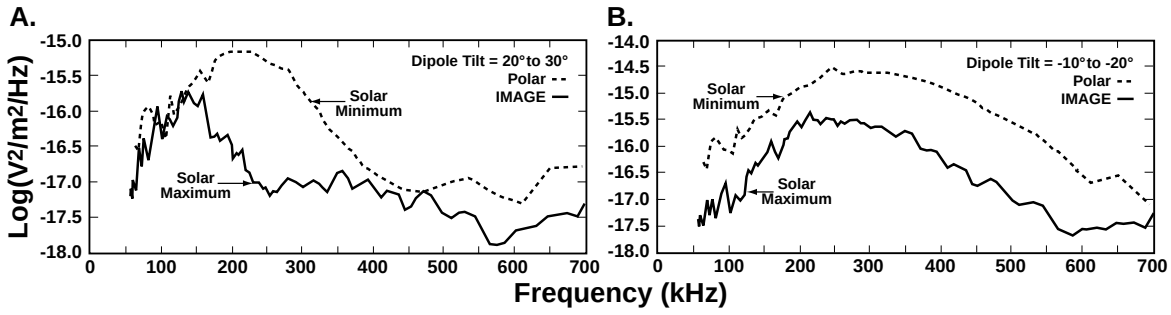

Figure 5: Comparison of the average spectra over the same dipole tilt ranges where the emission peak is approximately constant for both Polar/PWI (dash) and IMAGE/RPI (solid) for both (a) positive and (b) negative dipole tilt angle.

5 Conclusion

The results presented in this paper and elsewhere (see Green et al. [2004]) are compelling, showing that there are significant variations in the average AKR spectrum as a function of dipole tilt and with the solar cycle.

Since the number of geomagnetic storms and their intensities greatly increases with solar activity it is generally believed that AKR would be more intense during solar maximum. The AKR spectrum is the least intense and narrowest in overall frequency range during summer/solar maximum and most intense and broadest during winter/solar minimum, a somewhat surprising result based on previous perceptions.

A consistent picture has emerged in which ionospheric density enhancements from sunlight during both positive dipole tilt configurations and solar maximum produce significant effects in the AKR spectral structure, source location, and emission intensity. The observations imply that the main auroral density cavity moves upward in altitude and becomes less pronounced as the Earth's dipole tilt changes from extreme negative values to extreme positive values.

The average AKR spectrum at solar maximum has the same structure with dipole tilt as at solar minimum but is typically lower (by as much as 1 to 2 orders of magnitude). In addition it is found that for negative dipole tilt a broad AKR source region exists, ranging from $\sim$18 to $\sim$24 MLT, with peak emission coming from $\sim$20 MLT. In comparison, under positive dipole tilt conditions the source region narrows ($\sim$ 20 to $\sim$ 24 MLT) with peak emission at $\sim$22 MLT.

The expected increases in ionospheric densities (with positive dipole tilt and solar EUV increases during solar maximum) play a significant role in magnetospheric-ionospheric coupling by: (1) shortening the altitude range of the auroral plasma cavity, (2) confining the cavity to a smaller range of MLT and closer to midnight, and (3) decreasing the overall intensity of AKR by lessening the depth of the auroral density cavity.

Previous studies have found reasonable correlations between AKR and the AE substorm index. Recently, Kumamoto et al. [2005] using Akebono data determined the correlation between AKR and the AE index with respect to season and solar cycle. They attribute the observed variations in the best fit parameters to changes in the ionosphere influencing the AKR source region.

References

Benediktov, E. A., G. G. Getmansev, N. A. Mityakov, V. O. Rapoport, and A. F. Tarozov, Relation between geomagnetic activity and the sporadic radio emission recorded by the Elektron satellites, *Cosmic Research*, English Translation, **6**, 791, 1968.

Benson, R. F., and W. Calvert, ISIS–1 observations at the source of auroral kilometric radiation, *Geophys. Res. Lett.*, **6**, 479, 1979.

Bougeret, J.-L., M. L. Kaiser, P. J. Kellogg, R. Manning, K. Goetz, S. J. Monson, N. Monge, L. Friel, C. A. Meetre, C. Perche, L. Sitruk, and S. Hoang, Waves: The Radio and Plasma Wave Investigation on the Wind Spacecraft, *Space Sci. Rev.*, **71**, 231, 1995.

Calvert, W., The auroral plasma cavity, *Geophys. Res. Lett.*, **8**, 919, 1981.

Dunckel, N., B. Ficklin, L. Rorden, and R. A. Helliwell, Low frequency noise observed in the distant magnetosphere with OGO 1, *J. Geophys. Res.*, **75**, 1854, 1970.

Ergun, R. E., C. W. Carlson, J. P. McFadden, G. T. Delory, R. J. Strangeway, and P. L. Pritchett, Electron-Cyclotron Maser Driven by Charged-Particle Acceleration from Magnetic Field- aligned Electric Fields, *ApJ.*, **538**, 456, 2000.

Gallagher, D. L., and D. A. Gurnett, Auroral kilometric radiation: Time averaged source position, *J. Geophys. Res.*, **84**, 6501, 1979.

Green, J. L., D. A. Gurnett, and S. D. Shawhan, The angular distribution of auroral kilometric radiation, *J. Geophys. Res.*, **82**, 1825, 1977.

Green, J. L., S. Boardsen, L. Garcia, S. F. Fung, and B. W. Reinisch, Seasonal and solar cycle dynamics of the auroral kilometric radiation source region, *J. Geophys. Res. (Space Physics)*, **109**, A18, A05223, doi:10.1029/2003JA010311, 2004.

Gurnett, D. A., The Earth as a radio source: terrestrial kilometric radiation, *J. Geophys. Res.*, **79**, 4227, 1974.

Gurnett, D. A., A. M. Persoon, R. F. Randall, D. L. Odem, S. L. Remington, T. F. Averkamp, M. M. DeBower, G. B. Hospodarsky, R. L. Huff, D. L. Kirchner, M. A. Mitchell, B. T. Pham, J. R. Phillips, W. J. Schintler, P. Sheyko, and D. R. Tomash, The POLAR plasma wave instrument, *Space Sci. Rev.*, **71**, 597–622, 1995.

Hilgers, A., A. Roux, and R. Lundin, Characteristics of AKR sources: a statistical description, *Geophys. Res. Lett.,* **18,** 1493, 1991.

Kaiser, M. L., and R. G. Stone, Earth as an intense planetary radio source: Similarities to Jupiter and Saturn, *Science*, **189**, 285, 1975.

Kaiser, M. L., and J. K. Alexander, Terrestrial kilometric radiation 3. Average spectral properties, *J. Geophys. Res.*, **82**, 3273–3280, 1977.

Kasaba, Y., H. Matsumoto, K. Hashimoto, and R. R. Anderson, The angular distribution of auroral kilometric radiation observed by the GEOTAIL spacecraft., *Geophys. Res. Lett.*, **24**, 2483–2486, 1997.

Kumamoto, A., T. Ono, M. Iizima and H. Oya, Seasonal and solar cycle variations of the vertical distribution of the occurrencce probability of auroral kilometric radiation sources and of upflowing ion events, *J. Geophys. Res.*, **108**, doi:10.1029/2002JA009522, 2003.

Kumamoto, A., T. Ono, M. Iizima, Seasonal and solar cycle dependences of the correlation between auroral kilometric radiation and the AE index, *Adv. Polar Upper Atmos. Res.*, **19**, 10–20, 2005.

Kurth, W. S., T. Murata, G. Lu, D. A. Gurnett, and H. Matsumoto, Auroral kilometric radiation and the auroral electrojet index for the January 1997 magnetic cloud event, *Geophys. Res. Lett.*, **25**, 3027–3030, 1998.

Kurth, W. S., D. A. Gurnett, Auroral kilometric radiation integrated power flux as a proxy for AE, *Adv. Space Res.*, **22**, 73–77, 1998.

Kurth, W. S., M. M. Baumback, and D. A. Gurnett, Direction–finding measurements of auroral kilometric radiation, *J. Geophys. Res.*, **80**, 2764, 1975.

Lee, L. C., J. R. Kan, and C. S. Wu, Generation of auroral kilometric radiation and the structure of auroral acceleration region, *Planet. Space Sci.*, **28**, 703, 1980.

Murata, T., H. Matsumoto, H. Kojima, and T. Iyemori, Correlations of AKR index with Kp and Dst indices, in *Proc. NIPR Symp. Upper Atmos. Physics*, **10**, 64–68, 1997.

Pazamickas, K. A., J. L. Green, D. L. Gallagher, S. A. Boardsen, S. Mende, H. Frey, and B. Reinisch, Correlation Between Low Frequency Auroral Kilometric Radiation and Auroral Structures, Submitted to *J. Geophys. Res.*, 2005.

Reinisch, B. W., D. M. Haines, K. Bibl, G. Cheney, I. A. Galkin, X. Huang, S. H. Myers, G. S. Sales, R. F. Benson, S. F. Fung, J. L. Green, S. Boardsen, W. W. L. Taylor, J.-L. Bougeret, R. Manning, N. Meyer-Vernet, M. Moncuquet, D. L. Carpenter, D. L. Gallagher, P. Reiff, The Radio Plasma Imager investigation on the IMAGE spacecraft, *Space Sci. Rev.*, **91**, 319–359, 2000.

Shawhan, S. D., D. A. Gurnett, and D. L. Odem, The plasma wave and quasi-static electric field instrument (PWI) for Dynamics Explorer–A, *Space Sci. Rev.*, **5**, 535–550, 1981.

Tsyganenko, N. A., Modeling the Earth's magnetospheric magnetic field confined within a relaistic magnetopause, *J. Geophys. Res.*, **100**, 5599–5612, 1995.

Voots, G., D. A. Gurnett, and S.-I. Akasofu, Auroral kilometric radiation as an indicator of auroral magnetic disturbances, *J. Geophys. Res.*, **82**, 2259–2266, 1977.

Wu, C. S., and L. C. Lee, A theory of the terrestrial kilometric radiation, *Astrophys. J.*, **230,** 621–626, 1979.

Zarka, P., Radio emissions from the planets and their moons, in *Radio Astronomy at Long Wavelengths*, *Geophysical Monograph* **119**, edited by R. G. Stone, J.-L. Bougeret, K. Weiler, and M. Goldstein, American Geophysical Union, Washington, 167–178, 2000.